Hydrodynamic interactions in two dimensions

R. Di Leonardo,[1,*] S. Keen,[2] F. Ianni,[1,3] J. Leach,[2] M. J. Padgett,[2] and G. Ruocco[1,3]
[1]*CNR-INFM, CRS SOFT c/o Dipartimento di Fisica, Universitá di Roma "La Sapienza," I-00185, Roma, Italy*
[2]*SUPA, Department of Physics & Astronomy, University of Glasgow, Glasgow, Scotland*
[3]*Dipartimento di Fisica, Universitá di Roma "La Sapienza," I-00185, Roma, Italy*
(Received 5 April 2008; published 17 September 2008)

We measure hydrodynamic interactions between colloidal particles confined in a thin sheet of fluid. The reduced dimensionality, compared to a bulk fluid, increases dramatically the range of couplings. Using optical tweezers we force a two body system along the eigenmodes of the mobility tensor and find that eigenmobilities change logarithmically with particle separation. At a hundred radii distance, the mobilities for rigid and relative motions differ by a factor of 2, whereas in bulk fluids, they would be practically indistinguishable. A two dimensional counterpart of Oseen hydrodynamic tensor quantitatively reproduces the observed behavior, once the relevant boundary conditions are recognized. These results highlight the importance of dimensionality for transport and interactions in colloidal systems and proteins in biological membranes.

DOI: 10.1103/PhysRevE.78.031406 PACS number(s): 82.70.Dd, 68.15.+e, 83.10.Pp, 87.80.Cc

When governing a world of lower dimensionality, the laws of physics give rise to intriguing phenomena. The reduced number of spatial dimensions usually results in stronger and longer ranged correlations. One example of this is long range Coulomb correlations and electron-lattice interactions which give rise to peculiar electronic and structural phase transitions in system of low dimensionality [1]. In a similar way, fluid flow propagators, mediating hydrodynamic interactions between suspended bodies, have logarithmic tails in two dimensions [2], giving rise to strong dynamical correlations [3].

When two particles suspended in a viscous fluid approach each other, propagation of fluid flow results in hydrodynamic interactions. As a consequence, a particle's motion resulting from a given stimuli, strongly depends on the entire instantaneous spatial configuration. Hydrodynamic interactions tend to favour correlated motions where every particle can move within the "slip stream" of its neighbors [4]. This has consequences on many collective phenomena such as colloidal aggregation and gel formation where attractive interactions push to modify interparticle distances [5]. Moreover, particles are always subject to stochastic thermal forces whose effects may be strongly influenced by hydrodynamic interactions, as happens in polymer dynamics [6], or for protein conformational changes [7,8]. In three-dimensional bulk fluids, the strength of hydrodynamic coupling decays as the inverse interparticle distance. This long-range character makes hydrodynamic interactions quite effective in determining dynamical behavior and poses a number of numerical and theoretical challenges to the physical modeling of such phenomena.

The situation is even more dramatic when fluid flow is restricted to two-dimensions, such as in cell membranes or thin films, and flow fields decay logarithmically with distance. The problem of two-dimensional, single particle mobilities has received a lot of attention due to its relevance for Brownian motion in cellular membranes [9]. However, much less is known about the equally nontrivial and important role of many body hydrodynamic interactions in two-dimensional systems. In particular, due to the very long range tails in fluid flow propagators, far field behavior may have a profound influence on what happens at much shorter lengths, determining the strength of hydrodynamic couplings between nearby particles. Failing to recognize this, the precise form of hydrodynamic interactions in 2D still lacks a complete formal description. For example, the subtle role of finite size effects has lead to question the validity of dynamical scaling for two-dimensional (2D) polymers on the basis of an unphysical form of the 2D Oseen tensor [10]. Such claims have only recently been disproved [11] by explicitly taking into account the finite size of the simulation box.

We propose a form of the 2D Oseen tensor which explicitly accounts for all the different far field boundary conditions and validate it by direct experimental observation within optical tweezers. We are interested in determining particle motions under the action of an external force field. To the lowest order in hydrodynamic interaction (large enough interparticle distances), it is sufficient to know single particle quantities and in particular the mobility b and the far field Green's tensor $\mathbf{G}(\mathbf{r})$ describing flow propagation

$$\dot{\mathbf{R}}_i = b\mathbf{F}_i \tag{1}$$

$$\mathbf{u}(\mathbf{r}) = \mathbf{G}(\mathbf{r} - \mathbf{R}_i) \cdot \mathbf{F}_i, \tag{2}$$

where $\mathbf{u}(\mathbf{r})$ is the flow field produced by a force $\mathbf{F}_i$ applied to a particle located in $\mathbf{R}_i$.

In a many body system the velocity of the ith particle will be (within the superposition approximation) the sum of two contributions: the speed that it would have in the absence of other particles plus an "ambient" velocity obtained as the sum of all the fluid velocities independently produced at $\mathbf{R}_i$ by other particles located at $\mathbf{R}_j$:

$$\dot{\mathbf{R}}_i = b\mathbf{F}_i + \sum_{j \neq i} \mathbf{G}(\mathbf{R}_i - \mathbf{R}_j) \cdot \mathbf{F}_j. \tag{3}$$

*roberto.dileonardo@phys.uniroma1.it

In bulk three-dimensional fluids, b is the inverse Stokes drag $(1/6\pi\mu a)$ while $\mathbf{G}$ is the Oseen tensor [6] which, in Cartesian coordinates, reads

$$G_{3D}^{\alpha\beta}(\mathbf{r}) = \frac{1}{8\pi\mu r}\left[\delta_{\alpha\beta} + \frac{r^\alpha r^\beta}{r^2}\right]. \tag{4}$$

It is important to note that spatially confining the particles to two dimensions is not sufficient to observe the long range tails. It is essential that the momentum flow is similarly restricted on a two-dimensional plane. To this aim it is crucial that the bounding fluid has a much smaller viscosity than the film itself, a solid boundary would lead instead to hydrodynamic interactions decaying faster than in the 3D case [12]. If we neglect stresses produced by the fluid bounding the film (air in our case) then the variations of flow properties across the film are negligible and dynamics is governed by a two-dimensional Stokes equation

$$\mu\nabla^2\mathbf{u}(\mathbf{r}) - \nabla p(\mathbf{r}) = -\mathbf{F}\delta(\mathbf{r})/h. \tag{5}$$

When complemented by the incompressibility condition $\nabla\cdot\mathbf{u}=0$, Eq. (5) can be rewritten as a biharmonic equation and solved for the propagator [13]

$$G_{2D}^{\alpha\beta}(\mathbf{r}) = \frac{1}{4\pi\mu h}\left[\delta_{\alpha\beta}\left(\ln\frac{L}{r} - 1\right) + \frac{r^\alpha r^\beta}{r^2}\right]. \tag{6}$$

It is clear that the logarithmic term appearing in Eq. (6) precludes the possibility of determining the integration constant L by imposing a vanishing velocity at infinity. In contrast to previous derivations of Eq. (6) we have explicitly included the length scale L whose role has been overlooked in the past. The divergence of flow field actually signals the presence of a length scale beyond which some of the assumed approximations fails.

There are three approximations involved in the derivation of Eq. (5): (1) infinite size of the film, (2) negligible inertia, (3) negligible viscous drag on the interfaces. For each of them there is a length scale beyond which the solution in Eq. (6) is not self-consistent with the assumed approximation. For the first approximation, the length scale is clearly the actual size of the film L_1. Following [9] we can impose a frictionless boundary on a ring of radius L_1 and obtain the expression (6) for the propagator where $L=L_1$. For a stick boundary condition one gets $L=L_1/\sqrt{e}$ [14]. In the second case, the flow field propagated by Eq. (6) fails to satisfy the negligible inertia approximation when the distance r is of order $L_2=\mu/\rho U$, where ρ is the fluid density and U is the typical particle speed. However, inertial terms in the Stokes equation can be approximately taken into account by the Oseen method [15] and obtain a short distance $(r\ll L_2)$ expression for the propagator which is given by Eq. (6) with $L=4\exp[1-\gamma]L_2\simeq 6.1L_2$ (γ is the Euler-Mascheroni constant). At last, one can obtain from Saffman solution [9] that the momentum flow through film interfaces cannot be neglected for distances of the order of $L_3=h\mu/\mu'$ where h is the film thickness and μ, μ' are, respectively, the viscosities of the film and that of the bounding fluid. However, even in that case, expression (6) remains valid in the neighborhood $r\ll L_3$ when we replace L with $\exp[1/2-\gamma]L_3\simeq 0.9L_3$. When dealing with mesoscopic systems however, due to the very low Reynolds number involved, L_2 is usually very large, a few hundred meters in our case. L_3 can range from the micron scale to the macroscopic scale according to the ratio of bounding fluid and film viscosities. In the present case where $L_3\sim 0.1$ m, we expect that hydrodynamic interactions are dominated by the finite size of the membrane. The following discussion will remain valid even in other situations, provided one uses the relevant length scale L.

We can arrange all $\mathbf{R}_i$ in a single $2N$-dimensional vector and introduce the $2N\times 2N$ hydrodynamic mobility tensor $\mathbf{H}$ so that Eq. (3) reads

$$\dot{\mathbf{R}} = \mathbf{H}(\mathbf{R})\cdot\mathbf{F}, \tag{7}$$

$$H_{ij}^{\alpha\beta}(\mathbf{R}) = \delta_{ij}\delta_{\alpha\beta}b + (1-\delta_{ij})G^{\alpha\beta}(\mathbf{R}_i - \mathbf{R}_j). \tag{8}$$

We now have a two-dimensional expression for the propagator (6) that can be used in Eq. (8) to get the many-body mobility tensor. The effect of boundary conditions on the mobility tensor is condensed in the length L appearing in the logarithmic term of the propagator G. We will check the validity of our expression for $\mathbf{H}$ by observing the dynamical behavior of two colloidal particles confined in a free-standing liquid film. In a two body system, if we choose the x axis along the joining line, x and y dynamics are naturally decoupled for symmetry reasons. We can then decompose $\mathbf{H}$ into two 2×2 mobility tensors operating on the subspaces of x and y coordinates. Each of those 2×2 tensors is diagonal in the coordinate system of the two eigenvectors (1, 1) and (1, −1), corresponding, respectively, to a rigid translation and a stretching motion. Without losing any generality we can then assume that our mobility tensor is fully characterized by its four eigenvalues. Using expression (6) in Eq. (8) we can diagonalize the mobility tensor in the two-body case and obtain the four eigenvalues as a function of interparticle distance r:

$$\lambda_{x\pm} = b\left[1 \pm \frac{1}{4\pi\mu hb}\ln\frac{L}{r}\right], \tag{9}$$

$$\lambda_{y\pm} = b\left[1 \pm \frac{1}{4\pi\mu hb}\left(\ln\frac{L}{r} - 1\right)\right]. \tag{10}$$

As in the three-dimensional case, hydrodynamic interactions produce a splitting in the spectrum of mobilities by favouring rigid motions and opposing to relative displacements. The splitting is symmetric about the average single particle mobility and is larger for parallel than for perpendicular forcing. In three dimensions, the entity of the splitting decays as the inverse separation falling below 10% when particles distance grows beyond ten radii. The dependence on distance, in the two-dimensional case, occurs only through a logarithmic term, which makes hydrodynamic interactions practically unavoidable. Cheung and co-workers [3] used video microscopy to obtain evidence of long ranged spatial correlations between spheres floating in a free standing liquid film. However, many-body effects were found to

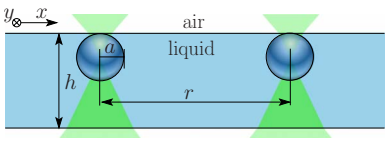

FIG. 1. (Color online) Trapping geometry. Two beads of radius a are optically trapped at a distance r in a liquid film of thickness h.

be significant even at very small concentrations, practically precluding the possibility of isolating hydrodynamic effects from indirect bulk measurements.

On the other hand, optical tweezers allow the positioning of two beads at varying separations, isolated from boundaries and other particles. The tweezers can also be used to simultaneously drive particles along any direction and directly probe the full mobility tensor. To this aim we disperse latex beads (2 μm diameter) in a water-glycerol mixture with 0.2 % wt sodium dodecyl sulfate (SDS) surfactant added. A thin film is obtained by sweeping the solution on a square frame (6 mm side) of nylon wires (60 μm thickness) [16]. Glycerol increases viscosity and slows down both drainage and evaporation, resulting in longer lived films. Starting with a 50 % wt water/glycerol film and then heating to evaporate most of the water, we can obtain a very viscous film with a few micron thickness. We measured the film thickness h at the beginning and at the end of the reported experiment to be 3.9 μm. Particles are imaged by a 40× NA 0.75 objective of an inverted optical microscope (Nikon TE2000-U). The same objective is used to focus the laser beam ($\lambda=532$ nm) diffracted off a spatial light modulator (SLM, Holoeye LCR-2500) into two, dynamically reconfigurable, optical traps [17,18]. Axial confinement is by capillary force on the top surface of the liquid film (Fig. 1).

In contrast to previous studies of hydrodynamic interactions in 3D [4,19,20], where eigenmobilities were extracted from the correlated fluctuations of optically trapped particles, we choose to measure the eigenmobilities by directly exciting the four eigenmodes. A pair of optically trapped particles is forced back and forth along each of the four eigenmodes (Fig. 2) by suddenly displacing the trap locations in the sample volume. The trap switch time is dictated by the SLM full refresh time (50 ms) which is much faster than the time scale of particle dynamics. As a consequence we can neglect particle motion during trap rearrangements and obtain an initial condition where particles are displaced from equilibrium positions (trap centers) along a specific eigencoordinate. Relaxation to the new equilibrium positions then occurs on different timescales for each of the four probed eigenmodes. In our experiment, external forces are of optical and stochastic origin:

$$\mathbf{F}_i = -k\delta\mathbf{R}_i + \mathbf{S}_i \tag{11}$$

with k the trap strength and $\delta\mathbf{R}_i=\mathbf{R}_i-\mathbf{R}_i^0$ the ith particle displacement from trap center $\mathbf{R}_i^0$. Assuming small displacements compared to interparticle distances and averaging over Brownian motion, we get from Eqs. (7) and (11)

$$\langle \delta\dot{\mathbf{R}} \rangle = -k\mathbf{H}(\mathbf{R}^0)\cdot\langle\delta\mathbf{R}\rangle. \tag{12}$$

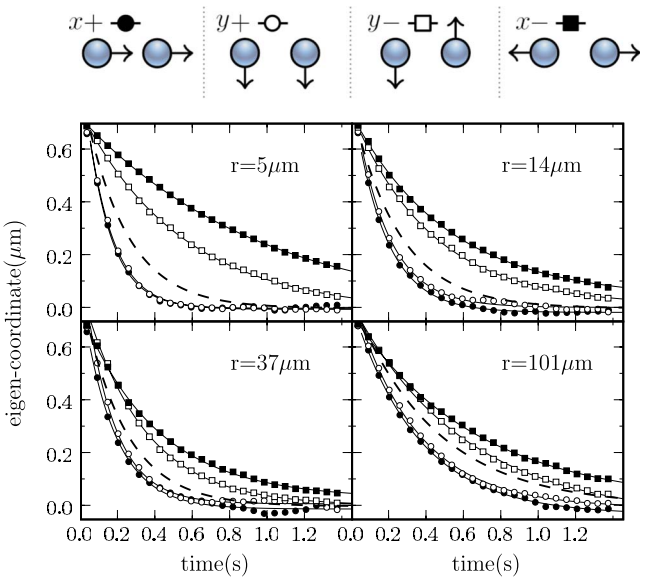

FIG. 2. (Color online) Relaxation of eigencoordinates. For each of the selected distances, we report the time evolution of the four eigencoordinates relaxing to equilibrium after the applied perturbation. Solid lines are exponential fits. Dashed line is the average, single particle dynamics.

If the initial configuration corresponds to a small displacement along the nth eigenmode $\langle\delta\mathbf{R}(0)\rangle=\epsilon\mathbf{e}_n$, then Eq. (12) has the solution

$$\langle\delta\mathbf{R}\rangle = \epsilon\exp[-k\lambda_n t]\mathbf{e}_n \tag{13}$$

and we can directly obtain the corresponding mobility λ_n by monitoring the amplitude of the $\mathbf{e}_n$ mode relaxing to equilibrium. We choose to normalize the eigenvectors such that the corresponding eigencoordinates give the center-of-mass position, for the rigid modes, and the half distance (along x or y) for stretching modes.

We choose ten logarithmically spaced interparticle separations between 5 and 100 μm and drive the two particles back and forth (eight times) along each of the four eigenmodes. Particle coordinates were digitally extracted from video frames at 144 Hz. Eigencoordinates were then computed and averaged over the eight iterations. Figure 2 shows the time evolution of the four eigencoordinates at four selected interparticle distances. The two x and y rigid motions are much more mobile than the corresponding stretching motions. This behavior remains clearly visible up to the highest investigated distance (100 particle radii). By fitting the eigencoordinate dynamics to the exponential law in Eq. (13) we can extract the four decay rates $k\lambda_n$ where the trap stiffness k only enters as a proportionality factor. To correct for variations in trap strength k, for each distance (fixed k), we normalize the four obtained rates to their average value removing any residual dependence on trap strength. The normalized rates directly correspond to the four normalized mobilities λ_n/b and are shown in Fig. 3 as a function of the particle separation. The strength of hydrodynamic coupling, reflected in the splitting of mobilities, decays logarithmically slow with distance. Even at a separation of 100 radii, par-

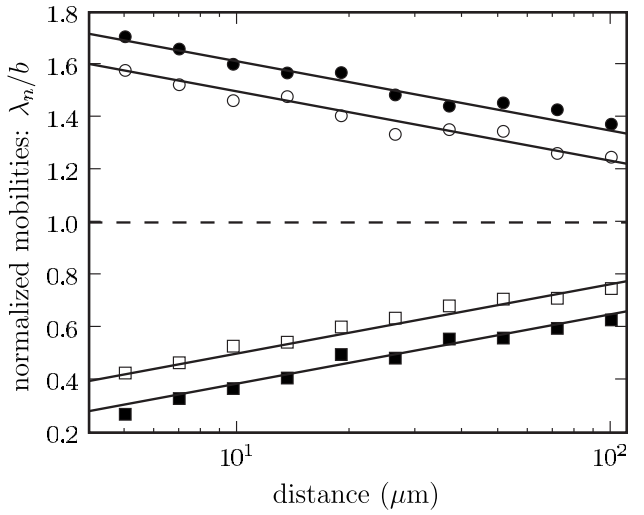

FIG. 3. Eigenmobilities. The four eigenmobilities of a two particle system arranged at different particles separations. To correct for variations in trapping power, for each distance mobilities have been normalized to their average.

ticles move twice as fast when forced along the same direction rather than in the opposite direction. At the same large separation, three-dimensional mobilities would only differ by 1%.

The four data sets in Fig. 3 can be very well fitted by Eq. (9) leaving L and the adimensional mobility $b^*=4\pi\mu hb$ as the only free parameters. We obtain as best fit parameters $b^*=8.7$ and $L=2.1$ mm, the corresponding fitting curves are shown as straight lines. As expected, the relevant length scale L is determined by the film finite size. In particular a sticky boundary condition on a ring inscribed in the film frame ($L_1=3$ mm) would give $L=1.8$ mm. For the same boundary condition, the single particle mobility b can be calculated for a cylinder of height h, the film thickness [14]. Using our particle radius a as the cylinder radius we obtain $b^*=\ln(L_1/a)-1=7.0$ which compares reasonably well with the corresponding fitted value. We do not expect the two values to be in better agreement since the mobility b depends on the details of the boundary conditions on the particle surface. We anticipate that, when moving to multiparticle systems, the mobility of long wavelength eigenmodes will diverge linearly with the number of particles, rather than logarithmically as in the 3D case. As a first consequence of that, we could transport, at the same speed, any number of beads, using the same total amount of laser power. Moreover, the crossover to underdamped propagating modes on a linear chain of trapped particles predicted in Ref. [20], could be experimentally verified much more easily.

We have directly measured hydrodynamic interactions between colloidal particles in a sheet of viscous fluid. The reduced dimensionality, compared to the bulk 3D fluids, results in stronger and longer ranged hydrodynamic couplings which are quantitatively reproduced by a two-dimensional version of the Oseen hydrodynamic tensor, once the relevant boundary conditions are recognized. The observed interactions constitute a general model for diffusion and interactions of proteins in biological membranes.

[1] P. W. Anderson, *Basic Notions of Condensed Matter Physics* (Perseus, New York, 1997).
[2] G. K Batchelor, *An Introduction to Fluid Dynamics* (Cambridge University Press, Cambridge, 1967).
[3] C. Cheung, Y. H. Hwang, X-l. Wu, and H. J. Choi, Phys. Rev. Lett. **76**, 2531 (1996).
[4] R. Di Leonardo, S. Keen, J. Leach, C. D. Saunter, G. D. Love, G. Ruocco, and M. J. Padgett, Phys. Rev. E **76**, 061402 (2007).
[5] H. Tanaka and T. Araki, Phys. Rev. Lett. **85**, 1338 (2000).
[6] M. Doi and S. F. Edwards, *The Theory of Polymer Dynamics* (Oxford University Press, Oxford, 1986).
[7] J. G. de la Torre and V. A. Bloomfield, Q. Rev. Biophys. **14**, 81 (1981).
[8] S. Hayward and N. Go, Annu. Rev. Phys. Chem. **46**, 223 (1995).
[9] P. G. Saffman, J. Fluid Mech. **73**, 593 (1976).
[10] S. R. Shannon and T. C. Choy, Phys. Rev. Lett. **79**, 1455 (1997).
[11] E. Falck, O. Punkkinen, I. Vattulainen, and T. Ala-Nissila, Phys. Rev. E **68**, 050102(R) (2003).
[12] B. Cui, H. Diamant, B. Lin, and S. A. Rice, Phys. Rev. Lett. **92**, 258301 (2004).
[13] C. Pozrikidis, *Boundary Integral and Singularity Methods for Linearized Viscous Flows* (Cambridge University Press, New York, 1992).
[14] J. Happel and H. Brenner, *Low Reynolds Number Hydrodynamics* (Kluwer Academic, Dordrecht, 1983).
[15] H. Lamb, *Hydrodynamics* (Cambridge University Press, Cambridge, 1932).
[16] R. Di Leonardo, F. Saglimbeni, and G. Ruocco, Phys. Rev. Lett. (to be published).
[17] J. E. Curtis, B. A. Koss, and D. G. Grier, Opt. Commun. **207**, 169 (2002).
[18] R. Di Leonardo, F. Ianni, and G. Ruocco, Opt. Express **15**, 1913 (2007).
[19] J. C. Meiners and S. R. Quake, Phys. Rev. Lett. **82**, 2211 (1999).
[20] M. Polin, D. G. Grier, and S. R. Quake, Phys. Rev. Lett. **96**, 088101 (2006).